BMC Plant Biology

RESEARCH Open Access

The viscoelastic properties of *Nicotiana tabacum* BY-2 suspension cell lines adapted to high osmolarity

Tomasz Skrzypczak[1*], Mikołaj Pochylski[2], Magdalena Rapp[3], Przemysław Wojtaszek[4] and Anna Kasprowicz-Maluśki[4]

Abstract

To survive and grow, plant cells must regulate the properties of their cellular microenvironment in response to ever changing external factors. How the biomechanical balance across the cell's internal structures is established and maintained during environmental variations remains a nurturing question. To provide insight into this issue we used two micro-mechanical imaging techniques, namely Brillouin light scattering and BODIPY-based molecular rotors Fluorescence Lifetime Imaging, to study *Nicotiana tabacum* suspension BY-2 cells long-term adapted to high concentrations of NaCl and mannitol. The molecular crowding in cytoplasm and vacuoles was examined, as well as tension in plasma membrane. To understand how sudden changes in osmolarity affect cellular mechanics, the response of the control and the already adapted cells to further short-term osmotic stimulus was also examined. The viscoelasticity of protoplasts is altered differently during adaptation processes compared to responses to sudden hyperosmolarity stress. The applied correlative approach provides evidence that adaptation to hyperosmotic stress leads to different ratios of protoplast and environmental qualities that help to maintain cell integrity. The viscoelastic properties of protoplasts are an element of plant cells long-term adaptation to high osmolarity. Moreover, such adaptation has an impact on the response to the hyperosmolarity stress.

*Correspondence:
Tomasz Skrzypczak
tskrzyp@amu.edu.pl

Full list of author information is available at the end of the article

Graphical Abstract

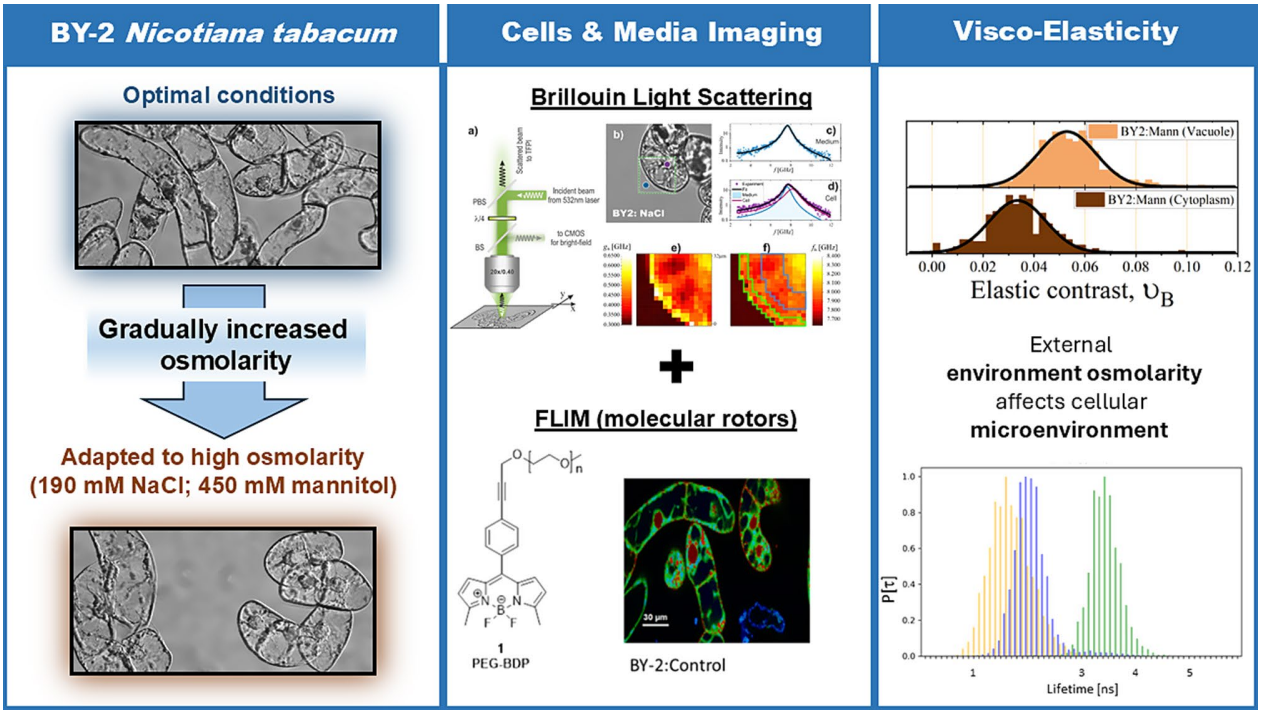

Keywords Plant cells, Osmotic stres adaptation, Molecular crowding, Viscoelasticity, Brillouin light scattering

Introduction

Understanding the interactions between the cellular microenvironment and the external environment remains a significant challenge in cell biology. One fundamental environmental factor with pleiotropic impacts is osmolarity, which can alter water activity and directly affect all cellular processes and biomechanics of a plants cell [72, 79]. Also in plants, during osmotic and salt stress signalling pathways are activated at first, leading to a quick stress response; in time, cells adjust their physiology, what include growth quiescence and recovery (reviewed in Julkowska & Testerink [28, 78]. In the case of salt stress, an excessive concentration of sodium is toxic, also by altering cation homeostasis (K^+/Na^+) and plasma membrane potential [36]. Additionally, also a high concentration of chloride anion is toxic and disturb anions homeostasis and consequently organellar physiology [19]. At the cellular level, established plants salt tolerance mechanisms include increased biosynthesis of osmolytes, cell wall remodelling, and intense export of Na^+ to vacuoles [16, 36, 68, 77].

Despite the vast information on the response to stress, it is still elusive how much changes in the biophysical properties of cells originate from the direct impact of an environment (i.e. passively imposed), and from the activity of cells in response to stress. Hyperosmolarity, as well as desiccation and temperature fluctuations, could severely alter water activity in cells, what disturbs cell growth, and entire molecular machinery, which necessitates reactions to overcome dysfunctions [56, 68, 72, 79]. Recent studies have demonstrated that hyperosmolarity stress rapidly increases cellular viscosity and molecular crowding in neuroblastoma cells [31]. Fundamentally, hyperosmotic stress leads to water efflux, hence increased molecular crowding (MC), that dramatically alters conditions crucial for cellular molecular machinery [56]. In plant cells a quick water efflux from a cell could induce temporal or irreversible plasmolysis.

The viscosity, which can also change due to hyperosmolarity, was shown to directly impact metabolism and enzymatic reactions [18, 31, 66]. The viscoelasticity per se has been indicated as an important factor in liquid-liquid phase separation processes in biological systems [63]. However, the viscoelastic properties of cells, although crucial for interactions between cells and environment, are much less studied than networks of signalling pathways and transcriptional response. It was shown, that in the mammalian cells, the cytoplasm behaves differently,

like liquid or like a gel, for molecules of different size. Importantly, the cytoplasmic viscosities were found to be similar across various cells lines [35]. The reason that the local viscosity and MC must be kept within a certain range is to clear the path for efficient diffusion [3]. In yeasts, it was shown that 'viscoadaptation' depends on the synthesis of glycogen and trehalose. Importantly, 'viscoadaptation' allows yeast cells to maintain efficient diffusion over a wide temperature range [51]. In HeLa cells, changes in cell volume in response to osmotic shocks are followed by changes in membrane tension, and such volume-membrane tension dynamics are actively regulated by the cell [55]. Recently, it was shown, that fundamentally for the stress response, biocondensates made of Intrinsically Disordered Proteins (IPDs) counteract microenvironmental instabilities induced by temperature and osmolarity changes [72].

The biomechanics of plant cells bases on the cell walls and vacuole driven turgor pressure. The turgor pressure and the bulk elastic modulus of a plant cell can be measured directly with a microcapillary invasive pressure probe [64]. A less-invasive approach for measuring elastic and viscoelastic properties of plant cells are indentation methods, based on the idea of measuring the force required to displace the surface of a sample by a given distance. The resulting force versus indentation curves can then be used to calculate the stiffness of a sample. These include atomic force microscopy (AFM) [42, 50, 58], cellular force microscopy (CFM) [57], microcompression [69, 70], and other single-point indentation systems [23, 37].

In the last decade many techniques have been developed and utilised to measure the mechanical properties of living biological materials, which enable also in situ measurements [13, 14, 31, 41, 53, 59, 74]. Cell microenvironment-sensing dyes based on fluorescence lifetime (FLIM) signals have proven to be robust and independent from concentration, precise in revealing cellular characteristics, such as pH, intrinsically disordered proteins status, redox status, hormone concentrations [8, 11, 31, 33, 43, 62, 67]. Importantly for plant biomechanics research, BODIPY-based fluorescent rotors were shown to be efficient tools in mapping viscosity with subcellular precision [41]. This toolbox has paved the way to explore in living cells how mechanical forces regulate biological processes, and vice versa.

Brillouin Light Scattering (BLS) was introduced as an all-optical contactless mechanical probe with diffraction-limited spatial resolution. This optical technique is based on the scattering of light on thermally generated acoustic waves that exist in any material. These waves acts as a mechanical stimuli, making material to effectively constantly deform itself, which allow to extract viscoelastic information from spectroscopic data. The property being directly measured in BLS, the frequency of the thermo-acoustic sound waves (so called Brillouin shift), is related to the refractive index, mass density and longitudinal elasticity modulus (Eq.S5). Although the relation between longitudinal modulus and more traditional Young's modulus is not direct, correlations between the two have been reported in several biological systems [54]. The dependence on the mechanical modulus makes BLS a fully non-invasive, label-free and contactless technique delivering mechanical information when physical access to the region of interest cannot be gained, such as in a cell or multicellular object [5, 13, 39]; Gouveia et al., 2019; Margueritat et al., 2019; Roberts et al., 2021; Wisniewski et al., 2020; Bevilacqua et al., 2023; Elsayad et al., [13]. The Brillouin frequency shift in biological materials is influenced by factors such as the intrinsic properties of individual components, their scale, cross-linking degree, local microenvironment compressibility, and the solid–liquid volume fraction. At the intracellular level, elasticity is governed by the cell's complex internal structure, particularly the cytoskeleton and liquid fraction. Proof-of-principle experiments have demonstrated that the Brillouin shift is sensitive to filament crosslinking and the solid–liquid volume fraction, while cell stiffness is notably affected by water efflux, which alters intracellular molecular crowding [22, 52]. Recent studies have extended the application of Brillouin microscopy to measure cell wall stiffness in plant roots (Bacete et al., 2022; McKenna et al., 2019) and to explore mechanical properties in hydrated materials [74], multicellular spheroids [75], and mechanical anisotropy [29] in living matter. Among the various factors, water efflux and its impact on intracellular molecular crowding emerge as particularly significant.

The tobacco (*Nicotiana tabacum*) BY-2 suspension cell line is a well-established model in cell biology and biotechnology research [25, 26, 30, 34, 49, 61]. The use of BY-2 allows for investigation of cells derived from relatively homogenous population, that live in homogenous environments (culture media). Previously, the salt adapted BY-2 were shown to be characterised by significant changes in transcriptome, proteome and cellular ultrastructure, that underlie the importance of ROS homeostasis and sodium compartmentalization [17]. Moreover, the excretion of arabinogalactan proteins was revealed as positive factor in salinity tolerance in BY-2 [49]. Here, we utilised BY-2 cell lines adapted to high concentrations of NaCl and mannitol. Gradual adaptations were performed as far as the highest tolerated concentrations were obtained, i.e. 190 mM NaCl for NaCl adapted BY-2 (BY-2:NaCl), and 450 mM mannitol for mannitol adapted BY-2 (BY-2:Mann). The analyzed in this research adapted cell lines presented significantly different morphologies and transcriptomes from the control cell line and from each other as well [60].

To address the question, whether adaptations had altered biomechanical properties of the cells, we performed micro-viscoelastic imaging on BY-2 suspension root cell line under various osmotic conditions. The utilisation of BODIPY(BDP)-based molecular rotors and BLS enabled us to reveal viscoelastic BY-2 properties with subcellular precision and by non-destructive methods. We analyzed cells exposed to high concentrations of NaCl or mannitol in the short-term ('stress') or long-term conditions ('adaptation') to establish a useful model to elucidate cellular responses to hyperosmolarity. Our results support the hypothesis that adjustment of cellular biomechanics to environmental conditions, contributes primarily to the cells long-term survival and makes a way for maintaining efficient metabolism.

Materials and methods

BY-2 cultures

Tobacco BY-2 suspension-cultured cells were maintained in liquid medium, pH 5.0, containing Murashige and Skoog salts (Murashige & Skoog 1962) and (per liter): 30 g sucrose, 100 mg inositol, 3 mg 2,4-D, 370 mg KH_2PO_4 and 1 mg thiamine-HCl (Nagata et al. 1992). Cells were subcultured weekly at 10 ml of culture per 70 ml of fresh medium in 300-mL Erlenmeyer flasks. Cultures were incubated at 21 °C on a gyratory shaker at 120 rpm with a 2.5-cm displacement. During 18 months, the cells were gradually adapted to grow in a media supplemented with either 450 mM mannitol (BY-2:Mann) or 190 mM NaCl (BY-2:NaCl). The cultures were transferred to fresh media containing increasing concentration of mannitol or NaCl in sequential manner, starting with 50 mM mannitol or 20 mM NaCl (osmotic agents concentrations were increased every 2 months), but were otherwise handled identically to the BY-2:Control cells. Immediately following transfer, the decrease intensity of cell divisions and decrease in the fresh weight of cells in culture were noted. However, after 4–8 subsequent passages, the adapted cells exhibited the same growth properties as control ones. This was usually considered appropriate the time point for the subsequent increase in the concentration of osmotic agent in culture media. Final concentrations of mannitol (450 mM) and NaCl (190 mM) were the highest that were not lethal to BY-2 cells. After the adaptation process, control and adapted cells were subcultured weekly to fresh media: control or media supplemented with either 450 mM mannitol (BY-2:Mann) or 190 mM NaCl (BY-2:NaCl). The osmolarities of fresh media without cells were measured with an osmometer. The highest media osmolarity was measured in the high mannitol adapted line (BY-2:Mann; ~750 mOsm/kg), than in the high NaCl adapted line (BY-2:NaCl; ~550 mOsm/kg). The lowest osmolarity was measured for the standard BY-2 medium used to culture BY-2:Control; ~220 mOsm/kg.

All the results described herein are from BY-2 cells subcultured to the media supplemented with the final concentrations of osmotic agents for at least 780 subcultures, and all the sampling and stress treatments were done on the third day (logarithmic growth phase) after transfer to fresh medium. For stress experiments, NaCl and mannitol were added to medium derived by centrifugation from the same day of culture. This allowed for minimising the effects of media compositions different from those of stress agents. To improve synchronization, cultures were kept for 2 weeks without subculture, followed by dilution of 5 ml of old culture in 70 ml of fresh medium. Undifferentiated and dividing cells were observed 2 days after that subculture, while differentiated non-dividing cells were observed after 10 days of culture.

For the mannitol and salt stress experiments BY-2 were centrifuged (300 RCF, 2 min.) and medium was exchanged to stress medium. To prepare medium for short-time stress treatments, 200 mM NaCl or 450 mM mannitol were added to medium derived by centrifugation from the same day of culture leading to final concentration of 200 mM NaCl or 450 mM mannitol for BY-2:Control, 390 mM NaCl or 450 mM mannitol for BY-2:NaCl, and 200 mM NaCl or 900 mM mannitol for BY-2:Mann. This cause that the only difference between stress media and culture media came from addition of stress agents. Cells were incubated with stress medium on shaker before imaging for time indicated.

Fluorescent BODIPY rotors synthesis

BODIPY-based (BDP) molecular rotors were synthesised according to a protocol described previously [41]. Procedure and NMR data results of synthesised rotors are available in Supplement: *SI_BDP_synthesis.pdf*.

BODIPY rotors imaging and data analysis

Cellular microviscosity was measured with BDP-based molecular rotor fluorescence probes in the middle days of the culture cycles. The cells were incubated with PEG-BDP for 1 h and with N^+-BDP for 3 h, and then washed twice with their respective culture media derived from a BY-2 culture. The PicoHarp300-Dual Channel SPAD system (PicoQuant) in combination with a Nikon A1Rsi microscope armed with the 20x dry or 60x /1.20 water immersion objective was used. The Picosecond Pulsed Diode Laser LDH-D-C-485 and Supercontinuum Tunable White Light Laser (488 nm) were used for generation of 100 ps excitation pulses at a repetition of 40 MHz. The images were of frame size of 256×256 pixels and were collected with an average count rate of around 10^5 photons per second for each apprx. 30–60 s, so that maximum photons per pixel reached 3 000 counts. FLIM

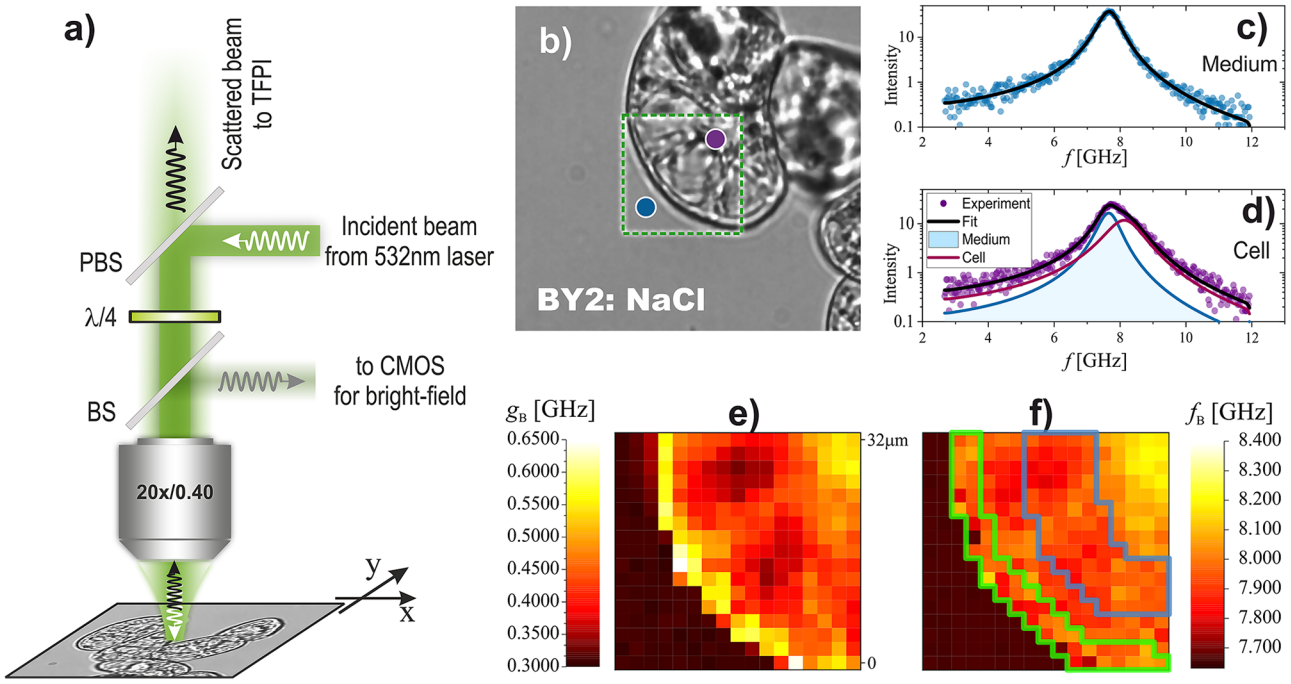

Fig. 1 Brillouin imaging of a cell. **a**) Schematic of the experimental setup for Brillouin micro-spectroscopy. BS, PBS, l/4 and l/2 stand, respectively, for removable beam splitter (for bright-field imaging), polarising beam splitter, quarter- and half-wave plates. **b**) Bright-field image of the cell. The green rectangle indicates the area chosen for Brillouin imaging. The blue and violet circles show the positions of the buffer and interior of the cell, respectively. **c**) Brillouin spectrum (anti-Stokes side) collected for buffer (Blue circle in **b**)). Notice that a single Brillouin peak is observed. **d**) Brillouin spectrum acquired inside the cell (violate circle in **b**)). Notice that the spectrum cannot be described by a single peak. Two peaks are necessary to reproduce the spectrum. One peak is assumed to come from scattering from a buffer (blue line). The second is a signal from the cell interior (dark red line). During spectrum fitting, the Brillouin peak parameters of the first peak were fixed to the values found for buffer. The Brillouin line shift and line width of the second peak (corresponding the cell) were mapped. **e**) Map of the Brillouin linewidth. **f**) map of the Brillouin lines shift. Green line border region identified in BF as cytoplasm dominating. Blue line border region identified in BF as vacuole dominating. The size of the maps is 32 µm

data were collected from more than 30 cells. Regions of Interest (ROI) were selected to mark properly subcellular compartments. Furthermore, the surrounding area of the cells was used to obtain a lifetime signal that revealed properties of the cells current environment. The fluorescence decay curves were fitted in each pixel with a best fitting decay model (single- or two-component exponential), and the lifetime mean and Standard Deviation were calculated. The lifetime signals distributions were assigned to 0.1 ns wide bins, then the all lifetime events occurrence were scaled in (0, 1) normalized range and plotted with matplotlib as histograms. Two sided Mann-Whitney test has been performed to obtain p-value for mean lifetime values.

Brillouin light scattering

In the Brillouin light scattering (BLS) experiment the incident laser beam from laser (Spectra Physics, Excelsior, l = 532 nm) was delivered to custom-built microscope of the usual design (Fig. 1a). The beam of vertical polarisation, reflected by the polarising beam-splitter, was passed through l/4 to produce incident beam of circular polarisation. The beam was focused on the sample with a 20x microscope objective (Zeiss LD Achroplan Korr; NA = 0.4). A low numerical aperture objective was used to reduce the spectral broadening effect [6] with the consequence of increasing the volume of scattering (6 × 20 µm). The sample was moved in the XY plane with a motorised translation stage (Märzhäuser Wetzlar GmbH & Co. KG). The power measured on the sample was 10 mW. The light backscattered from the sample was collected by the same objective and after restoring the vertical polarization (by passing through l/4) was transmitted by beam-splitter towards l/2 used to rotate polarization plane of scattered light before focussing on the entrance pinhole of the Brillouin spectrometer. For Brillouin spectrum measurement, Tandem Fabry-Perot Interferometer (TFPI) (TFP2, The Table Stable Ltd.) whose spectral range (FSR) was set to 15 GHz (10 mm mirror spacing).

The sample was sandwiched between two microscope slides. The starting position for XY scanning was chosen after inspection of the sample using bright-field imaging with the same microscope. At given XY position, recorded spectrum was average of 15 spectral sweeps giving ~ 10 s for single spectrum acquisition. Spectra

were collected for a 16 × 16 grid spaced by 2 µm. The total time to collect a single map was ~45 min. Each map was measured for a fresh sample.

In the investigation of cell mechanics, cells from every BY-2 line were extensively mapped, with more than 8 cells analysed for each line. The mapping process involved capturing bright field images to select specific regions showing bulk buffer, cell wall, and cell interior visibility, as illustrated in Fig. 1b.

Brillouin spectra analysis was conducted using single-phase or two-phase model (SI_BLS.pdf; Eq.S1), depending on whether the mapped area corresponded, respectively, to the bulk medium (Fig. 1c), or cell interior (Fig. 1d). The spatial distribution of the Brillouin line shift, f_B (informing about longitudinal elasticity), and the Brillouin line width, g_B (quantifying longitudinal viscosity), was visually represented in the form of maps (Fig. 1e, f), allowing for a comprehensive understanding of their variations across the cell. To enhance the analytical depth, manual selection of pixels was performed in each map, identifying three distinct regions: (1) medium (cell exterior/environment), (2) vacuole (interior of the cell, excluding nuclear region), and (3) cytoplasm (a protoplast in the vicinity of the cell wall).

Further insights into the viscoelastic properties of the cell and its environment were obtained through the production of histograms for f_B and g_B values. The parameters of the Brillouin line, such as shift and width, were examined for the three identified regions, providing a statistical overview of cellular mechanics and its surrounding medium. This multifaceted approach not only enabled a detailed analysis of individual cells, but also contributed to a broader understanding of the viscoelastic characteristics across different BY-2 lines.

Results

Adapted BY-2 lines exhibited unique properties of cytoplasmic molecular crowding

BDP-based cytoplasmic and plasma membrane (PM) based molecular rotors were used to obtain information on the viscosity of BY-2 subcellular compartments. The signals derived from PEG-BDP in the cytoplasm could be interpreted as an indicator of local molecular crowding (MC), while N^+-BDP works as a sensor of plasma membrane (PM) fluidity [41]. In the media, that is a liquid environment, PEG-BDP provided data that correspond to viscosity [41], so the cytoplasmic molecular crowding was presented relative to environmental viscosity.

PEG-BDP efficiently stained the cytoplasm of BY-2 cells and did not penetrate into vacuoles, but clearly diffused also to the nucleus (Fig. 2A). ROIs were used to isolate signals from the cytoplasm and to exclude denser nuclear areas. Lifetime was also measured in the medium area in cells vicinity (~50–100 µm from cells) to respect the impact of the real environment on the cellular microenvironment. This allowed the calculation relative of the differences between cells and their environment (Δ; *SI_BDPimage.pdf*). The lifetimes measured in the surrounding media were smaller than those measured inside the cells, and the lifetime distributions of the media were clearly distinguishable from those of the cells (Table 1).

The interior of the cells was expected to be denser and more viscous than the surrounding media. Indeed, it was already confirmed in BY-2:Control, in which lifetime of PEG-BDP was higher in the cytoplasm (t_c~2.1 ns), than in the media (t_e~1.69 ns). This translated to the relative difference (Δ) between the cytoplasm and the media around 24% (Table 1).

The adaptation to media of higher osmolarity requires that cells counteract the change and try to preserve intracellular conditions that allow for efficient diffusion and balance of water flow between a cell and an environment. Both adapted BY-2 lines displayed only slightly different PEG-BDP lifetime signals distributions, than did BY-2:Control. The distributions of lifetime values were slightly shifted toward higher lifetimes; +0.07–0.08 ns (Table 1). On the other hand, the relative to medium lifetime values (Δ) are much smaller in the both adapted BY-2 lines than in BY-2:Control. The lifetime signal distributions of the adapted cells were much closer to the media signals (Fig. 2). Moreover, the relative lifetime (Δ) of PEG-BDP in the cytoplasm was the highest in BY-2:Control (24%), followed by BY-2:Mann (20%) and BY-2:NaCl (12%) (Table 1). This effect was more manifested in lifetime distributions in media (t_e), than in cytoplasm (t_c) (Fig. 2).

Despite the fact that cells had been living in environment of higher osmolarity for many generations, the cytoplasmic molecular crowding remained almost stable. The smaller Δ in adapted BY-2:NaCl cells would have implied a cytoplasm of more similar density in comparison to environment, than in the case of BY-2:Control.

Interestingly, also cells from lines that were adapted and respectively subcultured to media supplemented with intermediate mannitol (250 mM, 350 mM) and NaCl (110 mM, 150 mM) concentrations exhibited very similar level of cytoplasmic MC, as lines adapted to the final concentrations. The constant MC level seems not to depend on osmolarity, if the adaptation to osmotic conditions had occurred (Supplementry Fig. 1).

Although, the t_e was the highest for BY-2:NaCl, it did not correspond to the measured media osmolarities, which was the highest for the BY-2:Mann media (Table 1). Because of the varied molecules' size and the electric charges, mannitol and NaCl might affect the osmolarity and viscosity of the medium differently. In two different environments with high osmolarity only slightly altered cytoplasmic MC were observed.

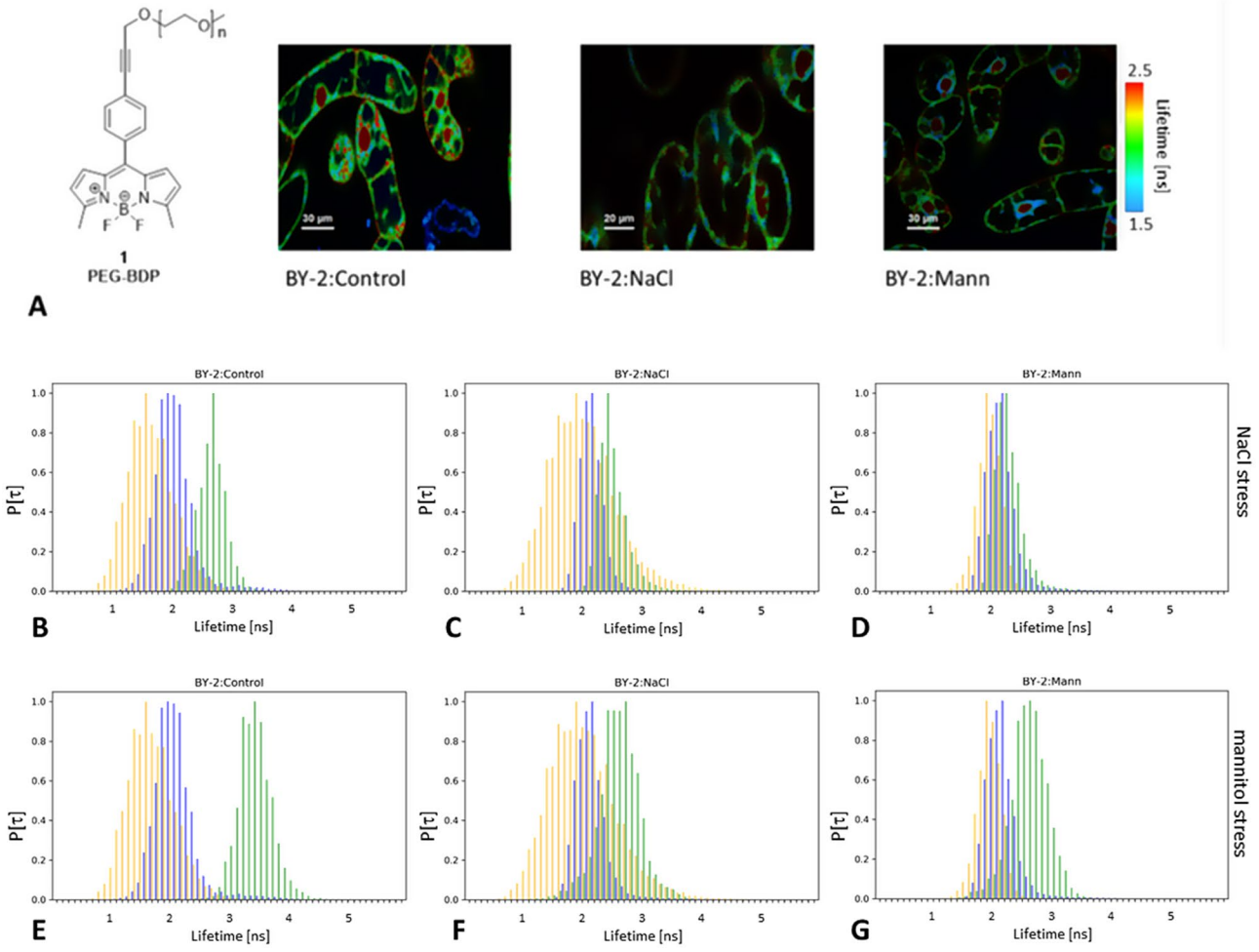

Fig. 2 **A**) PEG-BDP formula and images of PEG-BDP stained BY-2 lines. Lifetime BY-2 images are on a false colour scale that represents the mean lifetime for each pixel, expressed in nanoseconds. Nuclear regions with significantly higher lifetime values were not considered to determine the cytoplasmic lifetime and molecular crowd; **B**-**G**) Normalised distributions of the PEG-BDP lifetime derived from the cytoplasm (t_c) of the BY-2 lines. The cytoplasmic signal (blue) is plotted together with the medium signal (orange, t_e) derived from cell vicinities and the cytoplasmic signal for the stressed cells (green). (**B**-**D**) 200 mM NaCl stress; (**E**-**G**) 450 mM mannitol stress. **B**,**E**) BY-2:Control; **C**,**F**) BY-2:NaCl; **D**,**G**) BY-2:Mann

Table 1 Means and standard deviations (±) of lifetime PEG-BDP values derived from cytoplasm (t_c) of BY-2 cells and medium (t_e) in cells vicinity. The relative difference between cells and media was calculated and presented as Δ[%]. All values in ns. Asterisks denote significant differences between the value and t_c from the same BY-2 line. *$P < 0.1$, **$P < 0.01$

	Adapted			Stressed	
	t_c	t_e	Δ[%]: t_c vs. t_e	t_c NaCl stress	t_c mannitol stress
BY-2:Control	2.10 ± 0.13	**1.69 ± 0.15	**24%**	**2.67 ± 0.06	*3.40 ± 0.09
BY-2:NaCl	2.18 ± 0.04	**2.01 ± 0.33	**12%**	**2.48 ± 0.07	*2.59 ± 0.12
BY-2:Mann	2.17 ± 0.08	**1.81 ± 0.04	**20%**	**2.24 ± 0.07	**2.58 ± 0.10

Then, the osmotic stress response of BY-2 lines was determined. Increasing the NaCl concentration (+ 200 mM) led to the moderate level of plasmolysis within an hour of all BY-2 lines. Such salt stress resulted in significantly altered PEG-BDP lifetime distributions in BY-2:Control in a timeline below 30 min (Table 1; Fig. 2B-D). The t_c went significantly higher (t_c + 0.57 ns). This corresponds to an increase in MC in response to increased media osmolarity. The water efflux from the cells was induced. Similar, but more prominent trends (t_c + 1.3 ns), were observed after an application of 450 mM mannitol (Table 1). The addition of extra mannitol led to severe plasmolysis within all lines, so massive water leakage from cells also had occurred, what rapidly increased molecular crowding.

In both adapted lines increase in relative lifetime (Δ), as well as t_c increments were at least twice much smaller in adapted lines, than in BY-2:Control (Table 1).

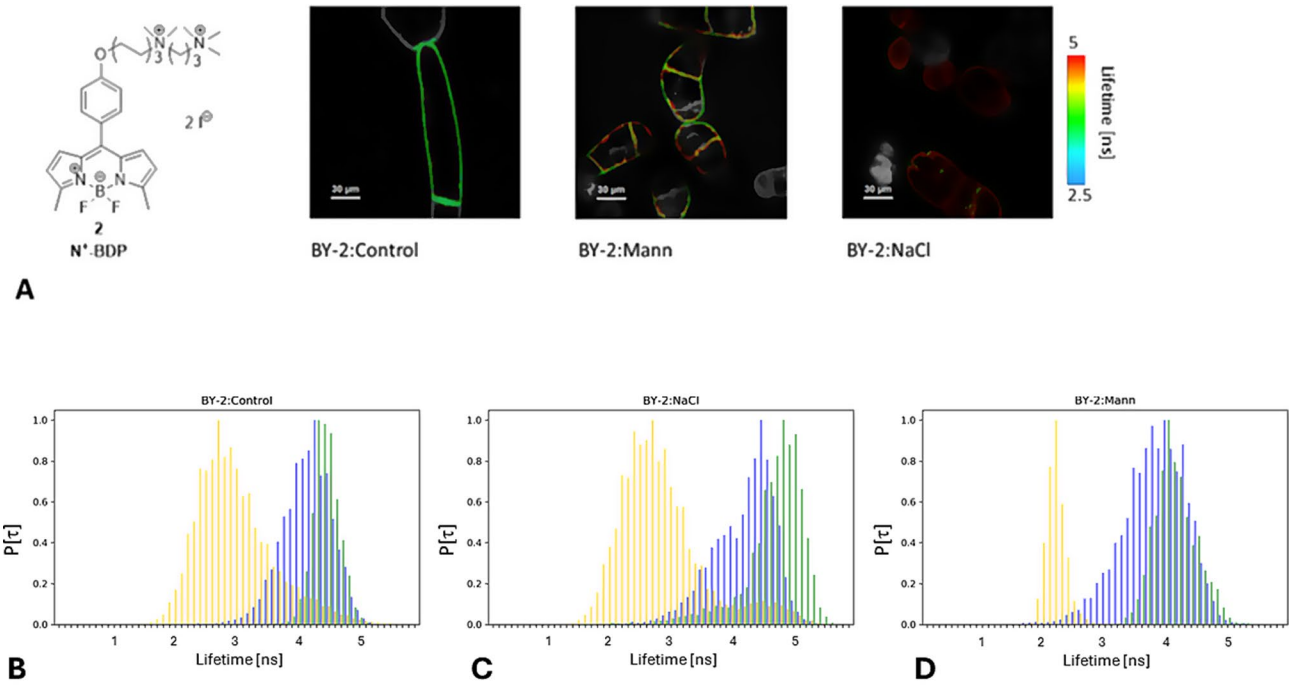

Fig. 3 **A**) N^+-BDP formula and N^+-BDP stained BY-2 lines. The images are on false colour scale, representing the mean lifetime for each pixel, expressed in nanoseconds. **B**-**D**) Normalised lifetime distributions of the N^+-BDP signal derived from the plasma membrane (t_m) of BY-2 lines (blue), which were subjected to additional NaCl stress (green). The plasma membrane signal is plotted on the background of the media signal derived from the vicinity of the cells (orange, t_{me}). **B**) BY-2:Control; **C**) BY-2:NaCl; **D**) BY-2:Mann

Table 2 Mean values and standard deviation (±) values of N^+-BDP lifetime values [ns] derived from plasma membrane (t_m) of BY-2 cells and medium (t_{em}) in cells vicinity. All values in ns. Asterisks denote significant differences between the value and t_m from the same BY-2 line. $*P<0.1$, $**P<0.01$

	Adapted		Stressed	
	t_m	t_{em}	t_m NaCl stress	t_m mannitol stress
BY-2:Control	4.16 ± 0.16	2.98 ± 0.41	*4.42 ± 0.06	3.50 ± 0.20
BY-2:NaCl	4.21 ± 0.25	2.85 ± 0.03	4.65 ± 0.25	3.98 ± 0.17
BY-2:Mann	3.82 ± 0.27	2.21 ± 0.50	**4.11 ± 0.12	n/a

MC increased the most in BY-2:Control, which lived in media of the lowest osmolarity and viscosity (the lowest t_e). Respectively, the changes were the smallest after stresses in BY-2:Mann, which were living in the media of the highest osmolarity (Fig. 2; Table 1). These smaller MC changes are consistent with the fact, that BY-2:NaCl and BY-2:Mann experienced relatively smaller increase in media osmolarity. Thus, we concluded, that after adaptation BY-2 maintained their basic properties of cytoplasm. However, MC changed less during response to osmotic stress.

Interestingly, the consecutive imaging of NaCl and mannitol stressed BY-2 cells showed that MC had changed immediately after hyperosmolarity stimulus, and then remained very stable in 2–35 min. timeline (Supplementary Fig. 2). This showed that cells are not able to restore initial MC level in short time and observed changes are results of water efflux forced by hyperosmolarity.

The preservation of the cytoplasmic microenvironment within some range seems to be required for cell survival and adaptation to high osmolarity. Furthermore, the cytoplasmic microenvironment after adaptation appears to make BY-2 cells less prone to osmotic stress-induced cytoplasm condensing.

Plasma membrane tension is similar within BY-2 cell lines

N^+-BDP rotor was shown to be an efficient tool for determining changes in plasma membrane tension (PM) [41]. In BY-2 heterogeneity of the lifetime within PM and intracellular membranes was observed (Fig. 3A). Increased N^+-BDP lifetime suggests decreased membrane tension.

The mean N^+-BDP lifetime in PM of BY-2:Control was 4.16 ns. The PM lifetime distribution and the lifetime mean value (4.21 ns) were slightly higher in BY-2:NaCl than in BY-2:Control. Surprisingly, BY-2:Mann exhibited a significantly lower t_m (3.82 ns), than BY-2:Control (Table 2). This would suggest an increase of the PM tension in the BY-2:Mann. However, also, osmotic stress invoked by 450 mM mannitol led to decreased t_m. Both, NaCl and mannitol stress led to PM detachment form cell walls (plasmolysis), and decreased PM tension was

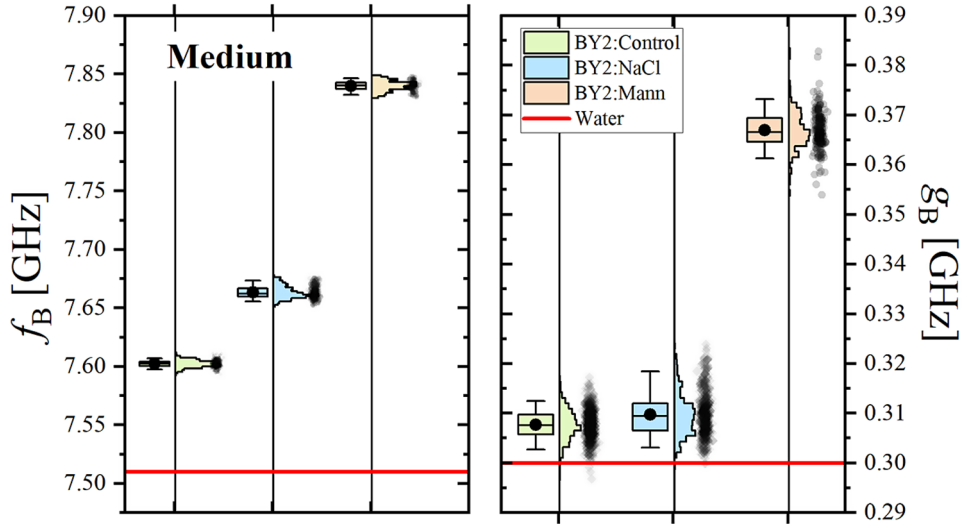

Fig. 4 Distributions of Brillouin line shift, fB, and linewidth, gB, for pure media. Horizontal red lines indicate values for bulk water

expected. It surprising is that, a longer lifetime was observed in the case of NaCl stress and a shorter lifetime in the case of mannitol stress (Table 2). Our results suggested that osmotic agent used for inducing hyperosmolarity could have an impact on rotors membrane tension indicators, so further research is required on rotors functioning in biological systems.

The t_m in PM of BY-2:Control cells after 200 mM NaCl stress was higher, than in the default medium (t_m + 0.26 ns). This implicates decreased PM tension that occurred in response to hyperosmolarity. This corresponds to observed moderate level of plasmolysis. N^+-BDP lifetime exhibited higher values also in the PM of BY-2:NaCl (t_m + 0.44 ns) and BY-2:Mann (t_m + 0.29 ns) in response to 200 mM NaCl stress (Table 2; Fig. 3B-D). Interestingly, BY-2:NaCl have the most altered N^+-BDP signals from plasma membranes after salt stress. This suggests that PM tension changed the most in salt stressed BY-2:NaCl. The base level of the t_m is slightly higher in BY-2:NaCl, also t_m in NaCl stress response is greater in BY-2:NaCl. We could speculate, that such effect depends on altered PM lipids composition.

Salt stress BY-2 lines stained with N^+-BDP were also imagined in a few minutes intervals with focus on the same cells. During 2–35 min. time course no significant changes were observed in N^+-BDP lifetime in cells plasma membrane. Hence, the most prominent changes in PM tension occurred immediately after hyperosmotic shock stimulus, when PM immediately being recoiled from cell walls (supplementary Fig. 3).

Our results suggest that through the adaptation process, the PM tension is maintained in BY-2:NaCl cells. Salt stress reduced PM tension in both BY-2:Control and the adapted ones, what correlates with plasmolysis and PM detachment from cell walls. Intriguingly, it is still to be resolved if maintaining biophysical characteristics in altered osmotic conditions required changes in PM lipids compositions.

Brillouin imaging revealed differences in viscoelasticity between BY-2:control and adapted lines

The distributions of the Brillouin line shift, $f_{B,\ medium}$, and linewidth, $g_{B,\ medium}$, for pure BY-2 media are presented in Fig. 4. The distributions of the media were narrow. Brillouin line shift and the linewidth for each medium were significantly higher than those observed in bulk water. The lowest values of both Brillouin measurable were found for BY-2:Control medium, a bit higher values correspond to BY-2:NaCl medium and the highest were found for BY-2:Mann medium. This result reflects the gradual increase in concentration and type of solutes in prepared culture media (BY-2:Control-> BY-2:NaCl-> BY-2:Mann).

Distributions of Brillouin line shift and line width for vacuole and cytoplasm dominating areas (Fig. 1f) are presented on Fig. 5. The distributions of those values are much broader (than those for pure media) being the joint result of inhomogeneity of cells and variations in cells properties. The values of both Brillouin parameters are distinctly higher than those found in pure media buffers. This is the manifestation of a trivial fact that cells were much more concentrated than liquid media. Significantly, if the cell lives in a buffer characterised by higher Brillouin line-shift (or linewidth), its protoplast is also characterised by higher Brillouin measurable. The cells become more crowded, if it is exposed to a more concentrated environment of higher osmolarity. In result: water is relatively more excreted from the cell, or cells produce more molecules to increase molecular crowd. However, it is hard to say which of the above two has the highest

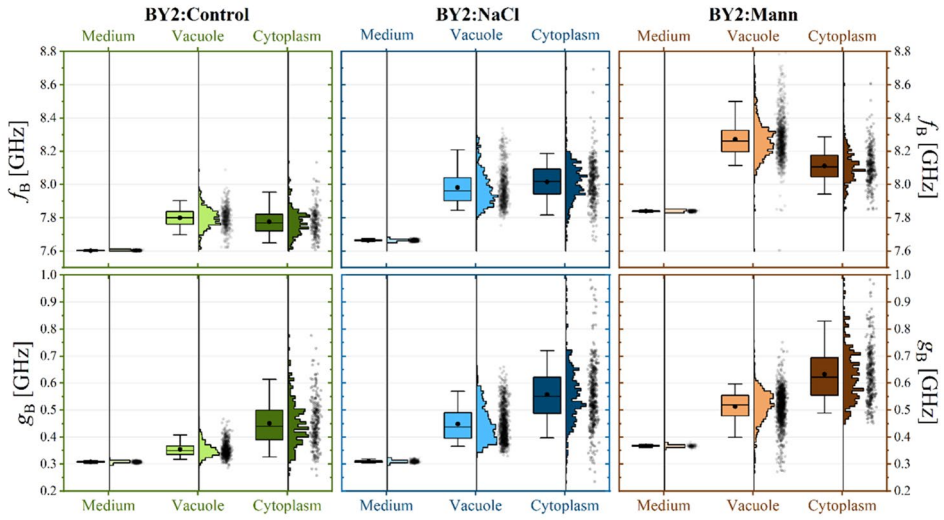

Fig. 5 Distributions of the Brillouin line shift, f_B,(upper panels) and Brillouin line width, g_B, (lower panels) for pure media, cell vacuoles and cytoplasm for three cell lines of cells (BY-2:Control– green, BY-2:NaCl– blue, BY-2:Mann– brown)

contribution, since Brillouin is measurable depending on quantity (concentration) and quality (specific compounds dissolved) [1, 75].

To better visualise the effect of medium on cell mechanical properties, Brillouin results were presented in the form of the relative to the medium Brillouin shift (named 'elastic contrast' in [7], υ_B, and the relative to the medium Brillouin line width ("viscous contrast"), γ_B, according to (*SI_BLS.pdf*; x7). It should be emphasised that the definitions of mechanical contrasts (elastic and viscous) adopted in this study differ from the usual ones [4], where changes in Brillouin line shape parameters are given in relation to the values characterising pure bulk water. We decided to express the contrasts relative to the media, as these are the natural environments of the examined cells. Such defined mechanical contrasts can be interpreted in terms of change of internal cells composition being the result of cells adaptation to different environments.

The distributions of elastic and viscous contrasts are presented in Fig. 6.

The BY-2 cell lines exhibited different Brillouin values υ_B and γ_B. Few interesting observations can be made from the data presented in Fig. 6, and Table 3. The distributions of elastic and viscous contrasts for the vacuoles are the narrowest for BY-2:Control cells, suggesting that these are the most homogeneous cells on both the population scales and the single cell scales. The relative Brillouin shift (elastic contrast) found for the vacuoles of the BY-2:Control cells was about 2.5% higher than its medium. For BY-2:NaCl cells it was about 4% higher, whereas for cells living in high mannitol, BY-2:Mann, the mean value was 5%. If we recall that the Brillouin shift depends on the compressibility of the system (which changes with molecules concentration), and if we accept that vacuoles can be treated as an aqueous mixture, then we can interpret this result as an indication of molecular crowding. The effect was specific for a given culture medium, which is the highest for BY-2:Mann, followed by BY-2:NaCl, and the lowest for BY-2:Control. A qualitatively similar trend is observed for the viscous contrast (relative Brillouin width) obtained for the vacuoles. Here, the mean values of the distributions starting from 13% for BY-2:Control cells, followed by 39% for BY-2:NaCl cells. The highest values of 43% were again observed for BY-2:Mann.

The above analysis of the distributions of elastic and viscous contrasts suggests that long-term exposure of cells to environments of concentrated NaCl and mannitol made the vacuoles more crowded and viscous. This effect was the most pronounced in BY-2:Mann. The result of molecular crowding was the reduction of the compressibility of the mixture and the increase in longitudinal viscosity. Brillouin values revealed variability in viscoelastic properties between cells adapted to various osmotic conditions. The elastic contrast values of vacuole are greater, than the elastic contrast values of cytoplasm. This effect was the most pronounced in BY-2:Mann. This might be consequences of the highest osmolarity to which were exposed BY-2:Mann, what might force the greatest mechanical rearrangements to maintain turgor and retain water.

Different results appeared when comparing the mechanical contrasts (both, elastic and viscous) recorded in cytoplasmic areas. Here, the highest values were found for BY-2:NaCl. Interestingly, BLS results showed that exposure to different culture media not only changed the overall composition of the cell, but also induced spatial

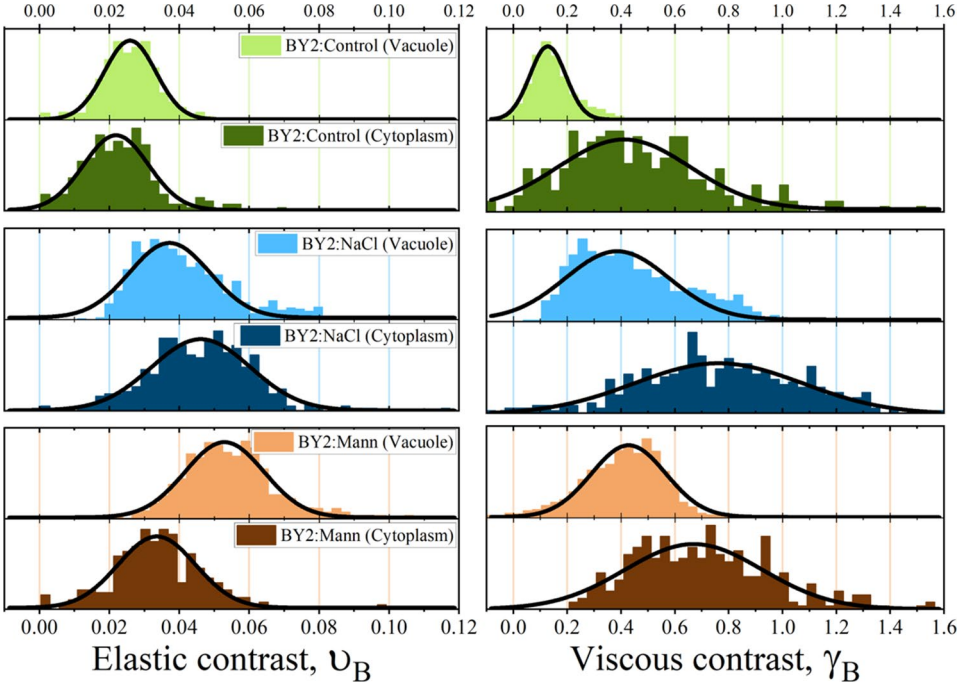

Fig. 6 Distributions of relative Brillouin shift fB, and relative Brillouin line width, gB, for vacuoles dominating areas and cytoplasm dominating areas for three cell lines of cells (BY-2:Control– green, BY-2:NaCl– blue, BY-2:Mann– brown)

Table 3 Elastic (u_B) and viscous (g_B) contrast values measured for different regions of the cells (cytoplasm and vacuole) belonging to three different lines. The values were obtained as a mean of the distribution (presented in Fig. 6 whereas the uncertainty (±) is the standard deviation

	u_B [%] (Elastic contrast)		g_B [%] (Viscous contrast)	
	Vacuole	**Cytoplasm**	**Vacuole**	**Cytoplasm**
BY-2:Control	2.59 ± 0.37	2.19 ± 0.93	12.79 ± 6.67	41.15 ± 24.55
BY-2:NaCl	3.72 ± 1.15	4.62 ± 1.42	38.59 ± 19.31	76.19 ± 31.34
BY-2:Mann	5.29 ± 1.13	3.36 ± 1.11	42.83 ± 13.83	67.00 ± 25.53

inhomogeneity of this composition. This was partially confirmed by the observation that cells exposed to NaCl showed the broadest and clearly asymmetric distributions of mechanical contrasts (elastic and viscous) being skewed toward higher values. BY-2:NaCl exhibited the most altered morphology [60]. In BY-2:NaCl medium, concentrated NaCl impose extra threat to cells, beyond osmolarity.

Our work also demonstrates the utility of BLS and fluorescent molecular rotors in investigating viscoelasticity in plant cells cultured under various osmotic conditions. As shown, correlating Brillouin spectroscopy with fluorescence microscopy would allow for correlating mechanical properties mapping with various subcellular structures. We suppose that BLS could become a very valuable tool for revealing cell reactions that involve alterations of the cellular microenvironment.

Discussion

Understanding the interrelations between a cellular microenvironment and an external environment remains a significant challenge in plants cell biology. One fundamental environmental factor with pleiotropic impact is osmolarity, which can rapidly alter water activity in cells, directly affect all cellular processes, and disturb biomechanical balance within plants cells elements [72, 79]. Plant cells sense the mechanical signals at the cell wall, plasma membrane and inside the cell. Information from these different cellular compartments is integrated to develop adaptive responses and maintain mechanical homeostasis at the cellular level [9, 20]. Although the significance of cell and tissue mechanics in plant development has been appreciated for many years [12, 44–46, 65], the study of cellular micromechanics at the level of the individual cell has proven to be problematic. The universal presence of the cellulosic cell wall and the apoplastic continuity that it provides endows plant tissues with a unique level of mechanical coupling. In principle, this makes it possible for plant tissues to transmit stress-mechanical information precisely and instantaneously over multicellular distances. However, the same apoplastic continuity that makes stress-mechanical signaling attractive as a possible developmental effector also makes it challenging to interpret responses and isolate mechanical variables at the level of the individual cell. Using individual cells cultivated in suspension helps control these variables, making it easier to interpret how cells respond

to a given environmental stimulus. Such model system allows to study plant biomechanical properties and their regulation by various extrinsic and intrinsic factors influenced by the physical interactions between cells and their environment [73].

Recent studies have demonstrated that in neuroblastoma cells hyperosmolarity rapidly increased cellular viscosity and molecular crowding [31]. Additionally, not only hyperosmolarity might boost MC– in microorganisms it was shown, that starvation leads to decreased cells size and increased molecular crowding [27]. The cytoplasmic viscosity in human cell lines was shown to be conserved across numerous cell lines, what indicates the importance of maintaining viscosity within a certain range [35]. On the other hand, the fibroblasts were characterized by higher cytoplasmic viscosity, that was reached by more dense ER network [35]. Our results highlights the potential of plant cells to maintain viscoelastic properties in the harsh environmental conditions, and only the slightly altered viscoelasticity of BY-2 cultures adapted to high osmolarity. The sudden hyperosmolarity stress induced changes were much greater, but also varied between lines. Hence, our studies underlie differences between impact of long- and short-term exposition to high osmolarity in the context of cells viscoelasticity and MC. The PEG-BDP rotors allowed us to discover a stable level of molecular crowding in cytoplasm of BY-2 lines. However, if considering differences between cytoplasm and environment lifetime (Δ), cytoplasm of BY-2:NaCl differed less in density from environment, than in BY-2:Control and BY-2:Mann. Interestingly, difference in environment might not be only due to different media recipes - the high NaCl adapted BY-2 were shown to modify their environment by increasing arabinogalactan proteins (AGP) excretion [49]. An intense secretion of macromolecules into cells exterior might has an impact on a local extracellular MC and a viscosity. For all lines we observed also the dynamic responses - the increased MC after osmotic stress. However, the adapted BY-2 exhibited smaller MC changes, than BY-2:Control. On the other hand, the BLS revealed that elastic contrast in the cytoplasm dominating areas was greater in adapted cells, than in BY-2:Control. Both results suggest distinguished molecular crowding specificity of BY-2:NaCl cytoplasm, that differ the most from BY-2:Control. The similarities and differences between data obtained with BLS and fluorescent molecular rotors require further research to point out, if they depend on various measured phenomenon, or properties of either media or cells. Relations between osmolarity, water activity, MC, viscosity, and ionic strength in cellular microenvironments are overlapping and interrelated, and challenging to elucidate in situ.

Vacuoles constitute a key component in plants cell osmoregulation, their content and mechanical properties are important for the stress response [2, 40]. How it could work a coordination between ions and water transport through PM and tonoplast, it has been proposed for guard cells [10]. By BLS we obtained data on approximate vacuoles areas, that were distinguished from cytoplasmic bands areas pushed to cell walls by vacuole's pressure. We did not have the possibility to integrate BLS with fluorescence microscopy, which would have allowed for a more precise identification of the subcellular compartment being measured. Both viscous and elastic contrasts are the greatest for vacuoles in BY-2:Mann. Such dense and viscous vacuoles correspond with the greatest osmolarity of BY-2:Mann medium. The high medium osmolarity impose adaptations, that would be concentrated on preventing water efflux and sustaining turgor.

We revealed interesting properties of measured by BLS elastic contrast in BY-2:NaCl. BLS revealed, that only in BY-2:NaCl molecular crowding seems to be higher in cytoplasm, than in vacuoles. It is tempting to speculate disturbed relations between biomechanics of vacuole and cytoplasm, that might lead to decreased size and altered shape of BY-2:NaCl cells. However, still more specific research on relation between vacuole and cytoplasm microenvironments is required to explain osmoadaptation and its consequences.

The utilized in this research NaCl and mannitol adapted BY-2 lines are characterized by different abiotic stress related gene expression patterns [60]. Moreover, both adapted cell lines successfully mitigated the prolonged risk of increased molecular crowding, membrane disintegration, and other disruptions triggered by hyperosmolarity stress. The identification of genetic factors that would determine the viscoelastic cellular traits and enable the efficient osmoadaptation could not be limited to a few regulators. However, in the recent research cell volume and PM tension coupling regulators have been identified [55]. Additionally, it is important to note that the impacts of NaCl on cells includes also sodium-specific toxicity and increased ionic strength, which can disturb the cellular microenvironment [24]. However, at some rate mannitol also increases ionic strength by inducing water efflux from cells, followed by a regulatory volume increase through the uptake of ions, and relative increase in ionic cellular constituents [79]. In future, advances in cellular biosensors of ionic strength could help to distinguish effects of ionic strength, ionic toxicity, and osmolarity/water activity on cells [38, 43].

Many questions remain to be answered regarding hyperosmolarity adaptation mechanisms. How do adapted BY-2 cells maintain efficient molecular machinery despite increased media osmolarity? Although osmoregulation mechanisms in plants have yet to be

fully elucidated, mechanosensitive channels likely play a crucial role in osmosensing [21, 47]. In animal cells, the detection of osmotic stress is associated with the activity of kinase ASK3 (MAP3K16), which depends on the location within poly(ADP-ribose) containing condensates, coupled with liquid-liquid phase separation and cascades of the signalling pathway [48, 71]. In plants, mono- and poly(ADP-ribosyl)ation was shown as involved in immunity, that often exhibits crosstalk with abiotic stress response [15, 32, 76].

Conclusions

In this paper, we presented and discussed the influence of varying environmental osmotic conditions on the viscoelastic properties of BY-2 cells long-term adapted to the elevated osmolarity. Fluorescent molecular rotors and Brillouin Light Scattering were innovatively used for analysis of viscoelasticity of living plants protoplasts with subcellular resolution. The stability of molecular crowding in cytoplasm and tension of plasma membrane correlated with long term suspension cell cultures survival and growth in environments of high osmolarities. Achieving such equilibrium in cellular microenvironment might be considered as the important element of osmoadaptation, that allow for long-term cells functioning and proliferation. On the other hand, the adaptation, resulted also in clear different properties of protoplasts, although molecular crowding and PM tension remain stable.

In a result of long-term osmoadaptation, the BY-2 lines altered their stress response, and exhibited smaller changes in cytoplasmic molecular crowding in reaction to the hyperosmolarity stress. Additionally, pioneering in the field of plants cell biology, the BLS analysis enabled us to reveal variations in the elastic and the viscous contrasts between BY-2 lines. Especially, the BY-2:Mann cells are characterised by the most crowded vacuoles, which correspond with the highest media osmolarity, what underlie the significance of vacuole driven turgor in the adaptation to the very high osmolarity. Despite many challenges that remained in the field of plant mechanobiology, our correlative approach provided deeper insight into plant cell responses to the environment and the further development of useful methods.

Supplementary Information

The online version contains supplementary material available at https://doi.org/10.1186/s12870-025-06232-3.

Supplementary Material 1

Supplementary Material 2

Acknowledgements
None.

Author contributions
P.W., A.K-M., and T.S. conceptualized the study. A.K-M performed BY-2 cell adaptation. T.S., M.P., and A.K-M. performed the experiments with BY-2 cells and analyzed the data. M.R. synthesized BDP-molecular rotors. T.S. and M.P. wrote the original draft, and A.K-M. reviewed the manuscript.

Funding
The work was supported by Polish National Science Centre (2020/39/B/NZ9/03336 and 2021/41/B/ST5/03038), by School of Sciences, Adam Mickiewicz University (Interdisciplinary research grant BNSNS023), by Inicjatywa Doskonałości - Uczelnia Badawcza (038/04/NP/0025).

Data availability
The experimental data is available upon reasonable request.The original BY-2 tobacco suspension cell line was derived from RIKEN National BioSource Project, Japan.

Declarations

Ethics approval and consent to participate
Nothing to declare.

Consent for publication
Nothing to declare.

Competing interests
The authors declare no competing interests.

Author details
[1]Center for Advanced Technology, Adam Mickiewicz University, Poznan, Poland
[2]Faculty of Physics, Adam Mickiewicz University, Poznan, Poland
[3]Faculty of Chemistry, Adam Mickiewicz University, Poznan, Poland
[4]Faculty of Biology, Adam Mickiewicz University, Poznan, Poland

Received: 21 October 2024 / Accepted: 10 February 2025
Published online: 25 February 2025

References

1. Adichtchev SV, Karpegina YA, Okotrub KA, Surovtseva MA, Zykova VA, Surovtsev NV. Brillouin spectroscopy of biorelevant fluids in relation to viscosity and solute concentration. Phys Rev E. 2019;99(6):062410. https://doi.org/10.1103/PhysRevE.99.062410.
2. Afzal Z, Howton TC, Sun Y, Mukhtar MS. The roles of aquaporins in plant stress responses. J Dev Biology (Vol. 2016;4. https://doi.org/10.3390/jdb4010009. Issue 1). MDPI Multidisciplinary Digital Publishing Institute.
3. Alfano C, Fichou Y, Huber K, Weiss M, Spruijt E, Ebbinghaus S, De Luca G, Morando MA, Vetri V, Temussi PA, Pastore A. Molecular crowding: the history and development of a scientific paradigm. Chemical Reviews. American Chemical Society; 2023. https://doi.org/10.1021/acs.chemrev.3c00615.
4. Antonacci G, Beck T, Bilenca A, Czarske J, Elsayad K, Guck J, Kim K, Krug B, Palombo F, Prevedel R, Scarcelli G, prevedel P. R. (2020). Recent progress and current opinions in Brillouin microscopy for life science applications. https://doi.org/10.1007/s12551-020-00701-9/Published
5. Antonacci G, de Turris V, Rosa A, Ruocco G. Background-deflection brillouin microscopy reveals altered biomechanics of intracellular stress granules by ALS protein FUS. Commun Biology. 2018;1(1):139. https://doi.org/10.1038/s42003-018-0148-x.
6. Antonacci G, Foreman MR, Paterson C, Török P. Spectral broadening in Brillouin imaging. Appl Phys Lett. 2013;103(22). https://doi.org/10.1063/1.4836477.
7. Bacete L, Schulz J, Engelsdorf T, Bartosova Z, Vaahtera L, Yan G, Gerhold JM, Tich T, Øvstebø C, Gigli-Bisceglia N, Johannessen-Starheim S, Margueritat J, Kollist H, Dehoux T, Mcadam SAM, Hamann T. (2021). THESEUS1 modulates cell wall stiffness and abscisic acid production in Arabidopsis thaliana.

Proceedings of the National Academy of Sciences, December 23, 2021 https://doi.org/10.1073/pnas.2119258119/
8. Colin L, Martin-Arevalillo R, Bovio S, Bauer A, Vernoux T, Caillaud M-C, Landrein B, Jaillais Y. Imaging the living plant cell: from probes to quantification. Plant Cell. 2022;34(1):247–72. https://doi.org/10.1093/plcell/koab237.
9. Cosgrove DJ. Wall extensibility: its nature, measurement and relationship to plant cell growth. New Phytol. 1993;124(1):1–23. https://doi.org/10.1111/j.1469-8137.1993.tb03795.x.
10. Cubero-Font P, De Angeli A. Connecting vacuolar and plasma membrane transport networks. New Phytologist. Volume 229. Blackwell Publishing Ltd; 2021. pp. 755–62. 2https://doi.org/10.1111/nph.16983.
11. Cuevas-Velazquez CL, Vellosillo T, Guadalupe K, Schmidt HB, Yu F, Moses D, Brophy JAN, Cosio-Acosta D, Das A, Wang L, Jones AM, Covarrubias AA, Sukenik S, Dinneny JR. Intrinsically disordered protein biosensor tracks the physical-chemical effects of osmotic stress on cells. Nat Commun. 2021;12(1). https://doi.org/10.1038/s41467-021-25736-8.
12. Echevin E, Le Gloanec C, Skowrońska N, Routier-Kierzkowska A-L, Burian A, Kierzkowski D. Growth and biomechanics of shoot organs. J Exp Bot. 2019;70(14):3573–85. https://doi.org/10.1093/jxb/erz205.
13. Elsayad K, Werner S, Gallemí M, Kong J, Guajardo ERS, Zhang L, Jaillais Y, Greb T. Mapping the subcellular mechanical properties of live cells in tissues with fluorescence emission-Brillouin imaging. Sci Signal 5 Jul 2016. 2016;9(435). https://doi.org/10.1126/scisignal.aaf6326. & Youssef Belkhadir, ¶
14. Farokh Payam A, Passian A. Imaging beyond the surface region: probing hidden materials via atomic force microscopy. Sci Adv. 2024;9(26):eadg8292. https://doi.org/10.1126/sciadv.adg8292.
15. Feng B, Liu C, de Oliveira MVV, Intorne AC, Li B, Babilonia K, de Souza Filho GA, Shan L, He P. Protein poly(ADP-ribosyl)ation regulates Arabidopsis Immune Gene expression and defense responses. PLoS Genet. 2015;11(1):e1004936. https://doi.org/10.1371/journal.pgen.1004936.
16. Flowers TJ, Colmer TD. Plant salt tolerance: adaptations in halophytes. Ann Botany. 2015;115(3):327–31. https://doi.org/10.1093/aob/mcu267.
17. Garciade la Garma J, Fernandez-Garcia N, Bardisi E, Pallol B, Asensio-Rubio JS, Bru R, et al. New insights into plant salt acclimation: the roles of vesicle trafficking and reactive oxygen species signalling in mitochondria and the endomembrane system. New Phytol. 2015;205(1):216–39. https://doi.org/10.1111/nph.12997
18. Gavish B, Werber MM. Viscosity-dependent structural fluctuations in enzyme catalysis. Biochemistry. 1979;18(7):1269–75. https://doi.org/10.1021/bi00574a023.
19. Geilfus CM. Chloride: from nutrient to toxicant. Plant Cell Physiol. 2018;59(5):877–86. https://doi.org/10.1093/pcp/pcy071.
20. Geitmann A, Ortega JKE. Mechanics and modelling of plant cell growth. Trends Plant Sci. 2009;14(9):467–78. https://doi.org/10.1016/j.tplants.2009.07.006.
21. Gorgues L, Li X, Maurel C, Martinière A, Nacry P. (2022). Root osmotic sensing from local perception to systemic responses. In Stress Biology (Vol. 2, Issue 1). Springer. https://doi.org/10.1007/s44154-022-00054-1
22. Guo M, Pegoraro AF, Mao A, Zhou EH, Arany PR, Han Y, Burnette DT, Jensen MH, Kasza KE, Moore JR, Mackintosh FC, Fredberg JJ, Mooney DJ, Lippincott-Schwartz J, Weitz DA. (2017). Cell volume change through water efflux impacts cell stiffness and stem cell fate. Proceedings of the National Academy of Sciences, 114(41). https://doi.org/10.1073/pnas.1705179114
23. Hayot CM, Forouzesh E, Goel A, Avramova Z, Turner JA. Viscoelastic properties of cell walls of single living plant cells determined by dynamic nanoindentation. J Exp Bot. 2012;63(7):2525–40. https://doi.org/10.1093/jxb/err428.
24. Honig B, Nicholls A. Classical Electrostatics in Biology and Chemistry. Science. 1995;268(5214):1144–9. https://doi.org/10.1126/science.7761829.
25. Hoque MA, Banu MNA, Okuma E, Amako K, Nakamura Y, Shimoishi Y, Murata Y. Exogenous proline and glycinebetaine increase NaCl-induced ascorbate-glutathione cycle enzyme activities, and proline improves salt tolerance more than glycinebetaine in tobacco Bright Yellow-2 suspension-cultured cells. J Plant Physiol. 2007;164(11):1457–68. https://doi.org/10.1016/j.jplph.2006.10.004.
26. Jelínková A, Müller K, Fílová-Parezová M, Petrášek J. NtGNL1a ARF-GEF acts in endocytosis in tobacco cells. BMC Plant Biol. 2015;15(1):1–14. https://doi.org/10.1186/s12870-015-0621-3.
27. Joyner RP, Tang JH, Helenius J, Dultz E, Brune C, Holt LJ, Huet S, Müller DJ, Weis K. (2016). A glucose-starvation response regulates the diffusion of macromolecules. eLife, 2016;5:e09376 https://doi.org/10.7554/eLife.09376.001
28. Julkowska MM, Testerink C. Tuning plant signaling and growth to survive salt. Trends Plant Sci. 2015;20(9):586–94. https://doi.org/10.1016/j.tplants.2015.06.008.
29. Keshmiri H, Cikes D, Samalova M, Schindler L, Appel L-M, Urbanek M, Yudushkin I, Slade D, Weninger WJ, Peaucelle A, Penninger J, Elsayad K. Brillouin light scattering anisotropy microscopy for imaging the viscoelastic anisotropy in living cells. Nat Photonics. 2024;18(3):276–85. https://doi.org/10.1038/s41566-023-01368-w.
30. Khatun M, Matsushima D, Rhaman MS, Okuma E, Nakamura T, Nakamura Y, Munemasa S, Murata Y. Exogenous proline enhances antioxidant enzyme activities but does not mitigate growth inhibition by selenate stress in tobacco BY-2 cells. Bioscience Biotechnol Biochem. 2020;84(11):2281–92. https://doi.org/10.1080/09168451.2020.1799747.
31. Kitamura A, Oasa S, Kawaguchi H, Osaka M, Vukojević V, Kinjo M. Increased intracellular crowding during hyperosmotic stress. Sci Rep. 2023;13(1). https://doi.org/10.1038/s41598-023-39090-w.
32. Kong L, Feng B, Yan Y, Zhang C, Kim JH, Xu L, Rack JGM, Wang Y, Jang J-C, Ahel I, Shan L, He P. Noncanonical mono(ADP-ribosyl)ation of zinc finger SZF proteins counteracts ubiquitination for protein homeostasis in plant immunity. Mol Cell. 2021;81(22):4591–e46048. https://doi.org/10.1016/j.molcel.2021.09.006.
33. Koveal D, Díaz-García CM, Yellen G. Fluorescent biosensors for neuronal metabolism and the challenges of quantitation. Curr Opin Neurobiol. 2020;63:111–21. https://doi.org/10.1016/j.conb.2020.02.011.
34. Kurusu T, Yamanaka T, Nakano M, Takiguchi A, Ogasawara Y, Hayashi T, Iida K, Hanamata S, Shinozaki K, Iida H, Kuchitsu K. Involvement of the putative ca 2+-permeable mechanosensitive channels, NtMCA1 and NtMCA2, in ca 2 + uptake, ca 2+-dependent cell proliferation and mechanical stress-induced gene expression in tobacco (Nicotiana tabacum) BY-2 cells. J Plant Res. 2012;125(4):555–68. https://doi.org/10.1007/s10265-011-0462-6.
35. Kwapiszewska K, Szczepański K, Kalwarczyk T, Michalska B, Patalas-Krawczyk P, Szymański J, Andryszewski T, Iwan M, Duszyński J, Hołyst R. Nanoscale viscosity of cytoplasm is conserved in human cell lines. J Phys Chem Lett. 2020;11(16):6914–20. https://doi.org/10.1021/acs.jpclett.0c01748.
36. Li J, Yang Y. How do plants maintain pH and ion homeostasis under saline-alkali stress? Front Plant Sci. 2023;14. https://doi.org/10.3389/fpls.2023.1217193.
37. Lintilhac PM, Wei C, Tanguay JJ, Outwater JO. Ball tonometry: a rapid, nondestructive method for measuring cell turgor pressure in thin-walled plant cells. J Plant Growth Regul. 2000;19(1):90–7. https://doi.org/10.1007/s003440000009.
38. Liu B, Poolman B, Boersma AJ. Ionic strength sensing in living cells. ACS Chem Biol. 2017;12(10):2510–4. https://doi.org/10.1021/acschembio.7b00348.
39. Mattana S, Caponi S, Tamagnini F, Fioretto D, Palombo F. Viscoelasticity of amyloid plaques in transgenic mouse brain studied by Brillouin microspectroscopy and correlative Raman analysis. J Innovative Opt Health Sci. 2017;10(06):1742001. https://doi.org/10.1142/S1793545817420019.
40. Maurel C, Tacnet F, Güclü* J, Güclü* G, Guern J, Ripoche P. (1997). Purified vesicles of tobacco cell vacuolar and plasma membranes exhibit dramatically different water permeability and water channel activity. In Plant Biology (Vol. 94).
41. Michels L, Gorelova V, Harnvanichvech Y, Borst JW, Albada B, Weijers D, Sprakel J. Complete microviscosity maps of living plant cells and tissues with a toolbox of targeting mechanoprobes. Proc Natl Acad Sci USA. 2020;117(30):18110–8. https://doi.org/10.1073/pnas.1921374117.
42. Milani P, Gholamirad M, Traas J, Arnéodo A, Boudaoud A, Argoul F, Hamant O. *In vivo* analysis of local wall stiffness at the shoot apical meristem in Arabidopsis using atomic force microscopy. Plant J. 2011;67(6):1116–23. https://doi.org/10.1111/j.1365-313X.2011.04649.x.
43. Miller RC, Aplin CP, Kay TM, Leighton R, Libal C, Simonet R, Cembran A, Heikal AA, Boersma AJ, Sheets ED. FRET analysis of ionic strength sensors in the Hofmeister series of salt solutions using fluorescence lifetime measurements. J Phys Chem B. 2020;124(17):3447–58. https://doi.org/10.1021/acs.jpcb.9b10498.
44. Moulia B, Bastien R, Chauvet-Thiry H, Leblanc-Fournier N. Posture control in land plants: growth, position sensing, proprioception, balance, and elasticity. J Exp Bot. 2019;70(14):3467–94. https://doi.org/10.1093/jxb/erz278.
45. Moulia B, Coutand C, Julien J-L. Mechanosensitive control of plant growth: bearing the load, sensing, transducing, and responding. Front Plant Sci. 2015;6(February):52. https://doi.org/10.3389/fpls.2015.00052.
46. Moulia B, Douady S, Hamant O. Fluctuations shape plants through proprioception. Science. 2021;372(6540). https://doi.org/10.1126/science.abc6868.

47. Mousavi SAR, Dubin AE, Zeng WZ, Coombs AM, Do K, Ghadiri DA, Keenan WT, Ge C, Zhao Y, Patapoutian A. PIEZO ion channel is required for root mechanotransduction in Arabidopsis thaliana. Proc Natl Acad Sci USA. 2021;118(20):1–27. https://doi.org/10.1073/pnas.2102188118.
48. Naguro I, Umeda T, Kobayashi Y, Maruyama J, Hattori K, Shimizu Y, Kataoka K, Kim-Mitsuyama S, Uchida S, Vandewalle A, Noguchi T, Nishitoh H, Matsuzawa A, Takeda K, Ichijo H. ASK3 responds to osmotic stress and regulates blood pressure by suppressing WNK1-SPAK/OSR1 signaling in the kidney. Nat Commun. 2012;3. https://doi.org/10.1038/ncomms2283.
49. Olmos E, De La Garma JG, Gomez-Jimenez MC, Fernandez-Garcia N. Arabinogalactan proteins are involved in salt-adaptation and vesicle trafficking in tobacco by-2 cell cultures. Front Plant Sci. 2017;8(June):1–14. https://doi.org/10.3389/fpls.2017.01092.
50. Peaucelle A, Braybrook SA, Le Guillou L, Bron E, Kuhlemeier C, Höfte H. Pectin-induced changes in cell wall mechanics underlie organ initiation in Arabidopsis. Curr Biol. 2011;21(20):1720–6. https://doi.org/10.1016/j.cub.2011.08.057.
51. Persson LB, Ambati VS, Brandman O. Cellular control of viscosity counters changes in temperature and energy availability. Cell. 2020;183(6):1572–e158516. https://doi.org/10.1016/j.cell.2020.10.017.
52. Prevedel R, Diz-Muñoz A, Ruocco G, Antonacci G. Brillouin microscopy: an emerging tool for mechanobiology. Nat Methods. 2019;16(10):969–77. https://doi.org/10.1038/s41592-019-0543-3.
53. Robinson M, Filice CT, McRae DM, Leonenko Z. Atomic force microscopy and other scanning probe microscopy methods to study nanoscale domains in model lipid membranes. Adv Physics: X. 2023;8(1):2197623. https://doi.org/10.1080/23746149.2023.2197623.
54. Rodríguez-López R, Wang Z, Oda H, Erdi M, Kofinas P, Fytas G, Scarcelli G. Network viscoelasticity from Brillouin spectroscopy. Biomacromolecules. 2024;25(2):955–63. https://doi.org/10.1021/acs.biomac.3c01073.
55. Roffay C, Molinard G, Kim K, Urbanska M, Andrade V, Barbarasa V, Nowak P, Mercier V, García-Calvo J, Matile S, Loewith R, Echard A, Guck J, Lenz M, Roux A. (2021). Passive coupling of membrane tension and cell volume during active response of cells to osmosis. Biophysics and Computational Biology Cell. November 16, 2021, 118 (47). https://doi.org/10.1073/pnas.2103228118
56. Romero-Perez PS, Dorone Y, Flores E, Sukenik S, Boeynaems S. (2023). When phased without water: biophysics of cellular desiccation, from biomolecules to condensates. In Chemical Reviews (Vol. 123, Issue 14, pp. 9010–9035). American Chemical Society. https://doi.org/10.1021/acs.chemrev.2c00659
57. Routier-Kierzkowska A-L, Weber A, Kochova P, Felekis D, Nelson BJ, Kuhlemeier C, Smith RS. Cellular force microscopy for in vivo measurements of plant tissue mechanics. Plant Physiol. 2012;158(4):1514–22. https://doi.org/10.1104/pp.111.191460.
58. Sampathkumar A, Krupinski P, Wightman R, Milani P, Berquand A, Boudaoud A, Hamant O, Jönsson H, Meyerowitz EM. Subcellular and supracellular mechanical stress prescribes cytoskeleton behavior in Arabidopsis Cotyledon pavement cells. ELife. 2014;3. https://doi.org/10.7554/eLife.01967.
59. Seelbinder B, Wagner S, Jain M, Erben E, Klykov S, Stoev ID, Krishnaswamy VR, Kreysing M. (2024). Probe-free optical chromatin deformation and measurement of differential mechanical properties in the nucleus. ELife, 13. https://doi.org/10.7554/eLife.76421
60. Skrzypczak T, Wojtaszek P, Kasprowicz-Maluśki A. Heterogenous transcriptomes of Nicotiana tabacum BY-2 suspension cell lines adapted to various osmoticum. Biorxiv Org. 2024. https://doi.org/10.1101/2024.04.24.590873.
61. Srba M, Černíková A, Opatrný Z, Fischer L. Practical guidelines for the characterization of tobacco BY-2 cell lines. Biol Plant. 2016;60(1):13–24. https://doi.org/10.1007/s10535-015-0573-3.
62. Steinbeck J, Fuchs P, Negroni YL, Elsässer M, Lichtenauer S, Stockdreher Y, Feitosa-Araujo E, Kroll JB, Niemeier J-O, Humberg C, Smith EN, Mai M, Nunes-Nesi A, Meyer AJ, Zottini M, Morgan B, Wagner S, Schwarzländer M. In Vivo NADH/NAD + biosensing reveals the dynamics of cytosolic redox metabolism in plants. Plant Cell. 2020;32(10):3324–45. https://doi.org/10.1105/tpc.20.00241.
63. Tanaka H. Viscoelastic phase separation in biological cells. Commun Phys. 2022;5(1). https://doi.org/10.1038/s42005-022-00947-7.
64. Tomos AD, Leigh RA. THE PRESSURE PROBE: a versatile tool in plant cell physiology. Annu Rev Plant Physiol Plant Mol Biol. 1999;50(1):447–72. https://doi.org/10.1146/annurev.arplant.50.1.447.
65. Trinh D-C, Alonso-Serra J, Asaoka M, Colin L, Cortes M, Malivert A, Takatani S, Zhao F, Traas J, Trehin C, Hamant O. How mechanical forces shape plant organs. Curr Biol. 2021;31(3):R143–59. https://doi.org/10.1016/j.cub.2020.12.001.
66. Uribe S, Sampedro JG. Measuring solution viscosity and its effect on enzyme activity. Biol Procedures Online. 2003;5(1):108–15. https://doi.org/10.1251/bpo52.
67. van der Linden FH, Mahlandt EK, Arts JJG, Beumer J, Puschhof J, de Man SMA, Chertkova AO, Ponsioen B, Clevers H, van Buul JD, Postma M, Gadella TWJ, Goedhart J. A turquoise fluorescence lifetime-based biosensor for quantitative imaging of intracellular calcium. Nat Commun. 2021;12(1):7159. https://doi.org/10.1038/s41467-021-27249-w.
68. van Zelm E, Zhang Y, Testerink C. Salt tolerance mechanisms of plants. Annu Rev Plant Biol. 2020;71:403–33. https://doi.org/10.1146/annurev-arplant-050718-100005.
69. Wang CX. Modelling the mechanical properties of single suspension-cultured tomato cells. Ann Botany. 2004;93(4):443–53. https://doi.org/10.1093/aob/mch062.
70. Wang L, Hukin D, Pritchard J, Thomas C. Comparison of plant cell turgor pressure measurement by pressure probe and micromanipulation. Biotechnol Lett. 2006;28(15):1147–50. https://doi.org/10.1007/s10529-006-9075-x.
71. Watanabe K, Morishita K, Zhou X, Shiizaki S, Uchiyama Y, Koike M, Naguro I, Ichijo H. Cells recognize osmotic stress through liquid–liquid phase separation lubricated with poly(ADP-ribose). Nat Commun. 2021;12(1). https://doi.org/10.1038/s41467-021-21614-5.
72. Watson JL, Seinkmane E, Styles CT, Mihut A, Krüger LK, McNally KE, Planelles-Herrero VJ, Dudek M, McCall PM, Barbiero S, Vanden Oever M, Peak-Chew SY, Porebski BT, Zeng A, Rzechorzek NM, Wong DCS, Beale AD, Stangherlin A, Riggi M, Derivery E. Macromolecular condensation buffers intracellular water potential. Nature. 2023. https://doi.org/10.1038/s41586-023-06626-z.
73. Weber A, Braybrook S, Huflejt M, Mosca G, Routier-Kierzkowska AL, Smith RS. Measuring the mechanical properties of plant cells by combining micro-indentation with osmotic treatments. J Exp Bot. 2015;66(11):3229–41. https://doi.org/10.1093/jxb/erv135.
74. Wu P-H, Aroush DR-B, Asnacios A, Chen W-C, Dokukin ME, Doss BL, Durand-Smet P, Ekpenyong A, Guck J, Guz NV, Janmey PA, Lee JSH, Moore NM, Ott A, Poh Y-C, Ros R, Sander M, Sokolov I, Staunton JR, Wirtz D. A comparison of methods to assess cell mechanical properties. Nat Methods. 2018;15(7):491–8. https://doi.org/10.1038/s41592-018-0015-1.
75. Yan G, Monnier S, Mouelhi M, Dehoux T. Probing molecular crowding in compressed tissues with Brillouin light scattering. Biophys Comput Biology. 2021. https://doi.org/10.1073/pnas.2113614119/.
76. Yao D, Arguez MA, He P, Bent AF, Song J. Coordinated regulation of plant immunity by poly(ADP-ribosyl)ation and K63-linked ubiquitination. Mol Plant. 2021;14(12):2088–103. https://doi.org/10.1016/j.molp.2021.08.013.
77. Zhao C, Zhang H, Song C, Zhu JK, Shabala S. Mechanisms of plant responses and adaptation to soil salinity. Innov. 2020;1(1):100017. https://doi.org/10.1016/j.xinn.2020.100017.
78. Zhu JK. Salt and drought stress signal transduction in plants. Annu Rev Plant Biol. 2002;53:247–73. https://doi.org/10.1146/annurev.arplant.53.091401.143329.
79. Zonia L, Munnik T. Life under pressure: hydrostatic pressure in cell growth and function. Trends Plant Sci. 2007;12(3):90–7. https://doi.org/10.1016/j.tplants.2007.01.006.

Publisher's note